PCCP

ROYAL SOCIETY OF CHEMISTRY

B2O3/SiO2 substitution effect on structure and properties of Na2O-CaO-SrO-P2O5-SiO2 bioactive glasses from molecular dynamics simulations

SCHOLARONE™
Manuscripts

B₂O₃/SiO₂ substitution effect on structure and properties of Na₂O-CaO-SrO-P₂O₅-SiO₂ bioactive glasses from molecular dynamics simulations

Mengguo Ren, Xiaonan Lu, Lu Deng, Po-Hsuen Kuo, Jincheng Du*

Department of Materials Science and Engineering, University of North Texas, Denton, Texas, USA

(*Corresponding author. Email: du@unt.edu)

Abstract

The effect of B_2O_3/SiO_2 substitution in SrO containing 55S4.3 bioactive glasses on glass structure and properties such as ionic diffusion and glass transition temperature was investigated by combining experiments and molecular dynamics simulations with newly developed potentials. Both short-range (such as bond length and bond angle) and medium-range (such as polyhedral connection and ring size distribution) structures were determined as a function of glass composition. The simulation results were used to explain experimental results of glass properties such as glass transition temperature and bioactivity. The fraction of bridging oxygen linearly increased with increasing B_2O_3 content, resulting in an increase of overall glass network connectivity. Ion diffusion behavior was found to be sensitive to glass composition changes and trend of change with the level of substitution is also temperature dependent. The differential scanning calorimetry (DSC) results show a decrease of glass transition temperature (T_g) with increasing B_2O_3 content. This is explained by the increase of ion diffusion coefficient and decrease of ion diffusion energy barrier in glass melts as suggested by high temperature range (above T_g) ion diffusion calculation as B_2O_3/SiO_2 substitution increases. At low temperature range (below T_g), the E_a for modifier ions were increased with B_2O_3/SiO_2 substitution, which can be explained the increase of glass network connectivity. Vibrational density of states (VDOS) were calculated and show spectra feature changes as a result of the substation. The change of bioactivity with B_2O_3/SiO_2 substitution was discussed with the change of pH value and release of boric acid to the solution.

Key words: B_2O_3 substitution; MD simulation; bulk glass structure; diffusion

Graphical Abstract:
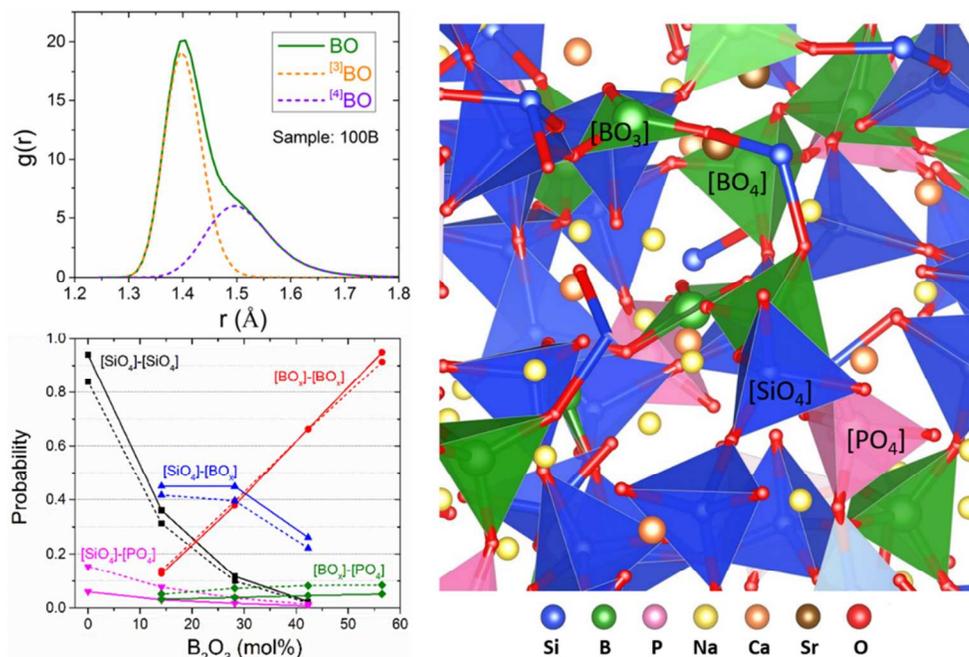
1. Introduction

It has been nearly 50 years since the first bioactive glass 45S5 and the Bioglass® family invented by Prof. Larry Hench in 1969.[1] The term "bioactive" was original referred to the ability of forming bonds with bone. With development of bioactive glasses (BG), a modified definition "stimulation of a beneficial biological response" was later proposed by Jones to account for various emerging applications.[2] During these years, various BG were investigated, and most of them are silica-based glasses. 45S5 Bioglass has high hydroxyapatite (HAp) formation rate, and can bond to both bone and soft tissue in vivo, making it one of the most bioactive glass composition ever studied. It is generally accepted that higher silica content in glass leads to a decrease of bioactivity. For glass with 52~60 wt% SiO_2, bonding is only to bone but not soft tissue. Melt-derived glasses with more than 60 wt% SiO_2 are usually considered to be bioinert (without bonding to bone and soft tissue).

Apart from extensive studies of silica-based bioactive glasses, borate glasses and phosphate glasses have also been explored as biomaterials. Borate-containing bioactive glasses have been

2

actively studied recently due to their promising clinical application in soft tissue repair and wound healing.[3,4] The initial stage of wound healing requires the formation of a fibrin clot. It is reported that borate based bioactive glass 13-93B3 (with composition of $53B_2O_3$-$20CaO$-$12K_2O$-$6Na_2O$-$5MgO$-$4P_2O_5$ in wt%) can be formed into microfibers with diameters ranging from 0.3 to 5 micrometers (μm) and have similar structure to the fibrin clot that can lead to wound healing.[3] Due to the flexible and cotton-like touch, such bioactive borate glass fibers can be applied to treat open wounds.[4]

Traditional studies of BG have focused on orthopedic applications for bone regeneration.[5–7] Several studies in the last decade have shown that certain borate glass compositions can be converted into HAp through a dissolution-precipitation process similar to that for silicate bioactive glass. [8,9] As compared to silicate glasses, it was found that borate glasses can be converted to HAp more completely and with more controllable rate when placed in K_2HPO_4 solution.[8,9] Previous studies also have shown borate BG are biocompatible and can enhance new bone formation.[10,11] Bi et al.[12] studied the effect of bioactive borate glass microstructure on bone regeneration. Scaffolds with three different microstructures: trabecular, oriented, and fibrous were compared in a rat calvarial defect model for 12 weeks. The results indicated that trabecular scaffolds showed better new bone formation, osteoinductive ability, as well as blood vessel infiltration, and thus may be more promising in bone repair.[12]

Dissolution of borate or borosilicate glasses, however, leads to the release of borate (BO_3^{3-}) ions, which may have negative effects on cell proliferation at too a high concentration. In vitro cell culture study has shown that borate ion concentrations of 2 mM (~22 μg/ml) produced a reduction in MC3T3-E1 cell density of around 40%.[13] Therefore, the potential toxicity of high concentrations of boron is a major concern for the application of borate BG implants. It is hoped that the 'dynamic' living body environment could effectively dilute local boron concentration, and thus alleviate the toxic effect on cells and tissues.[14] Zhang et al. studied the concentration of boron in serum as a function of implantation time of teicoplanin-loaded borate BG pellets in a rabbit tibia osteomyelitis model. The results showed that boron concentration increased to the highest value (~10 μg/ml) at 24 hours post implantation and fell into the level (~3 μg/ml) for healthy rabbits within 7-10 days, indicating that the released boron had no toxic effects to cells and tissues in vivo.[15]

Another possible application of borate-based bioactive glass is *in situ* drug delivery. Various BG or BG/polymer composites have been studied as potential drug delivery system.[14,16–19] As compared to silicate bioactive glass, the degradation of borate based bioactive glass is much faster and more complete. Also, the rate of degradation can be adjusted by controlling borate content in glass. Recently, an injectable borate bioactive glass cement was studied as a carrier for antibiotic vancomycin to cure osteomyelitis.[20] In vitro results have shown that adding borate bioactive glass in the cement provided a more sustained release of vancomycin into phosphate-buffered saline (PBS). In an *in vivo* study, a rabbit tibia osteomyelitis model was used to validate the capacity of borate bioactive glass cement to cure osteomyelitis and to regenerate bone.[20] Porous or hollow structure made of borate-based BG was explored due to their efficiency on ensuring homogeneous distribution of the drug through the matrix by controlling the release of drug.[21,22]

The difference of dissolution rate of borate and borosilicate glasses as compared to silicate glasses originates from different reaction rates of network linkages with water, where boron related network linkages are more easily attached by reaction with water than those for silicon. First principles calculations showed that the reaction energy barriers decrease in the sequence of Si-O-Si, Si-O-B and B-O-B linkages, which explains higher dissolution rate of borate containing glasses.[23] It was also found that three-fold coordinated boron reacts more easily with water than four-fold coordinated boron (e.g. reedmergnerite or danburite unites).[24,25] Hence understanding the atomic structure, especially the glass network structure and their connectivity, is critical to understand properties such as glass dissolution and bioactivity.

Despite wide biomedical applications of boron containing bioactive glasses, there are relatively little understanding of the structures of these glasses, especially the effect of boron oxide/silica substitution on the short and medium range structure features. These structure features are important to understand both the physical properties and, importantly, bioactivity as a function of glass composition. Thorough investigation of the structural details of these glasses is much needed but this is hindered by the amorphous nature and difficulties to fully characterize the atomic structures of these glasses.

Molecular dynamic (MD) simulations, which can provide both structural and dynamical properties, represents a powerful tool that complements experimental investigations to study the structure of complex bioactive glasses and to understand how properties (such as bioactivity)

depend on the glass structure and composition. *ab initio* MD (AIMD), where interatomic interactions are calculated from first principles, is an accurate and versatile approach that can be used to study various types of material systems and reactions of the glass surface with the water. However, high computational cost of AIMD limits the model size and accessible time scales, which makes exploration of medium-range glass structure features and long-time dynamic events unrealistic.[26] Using well developed reliable force field, classical MD can produce models of much larger size with more realistic short and medium range structures, which are particularly suitable for studies of multicomponent bioactive glasses. Du et al. studied the effect of SrO/CaO substitution on the structure, ionic diffusion and dynamic properties of 45S5 bioactive glass using MD simulation with a set of partial charge potentials and the results suggested the increase of dissolution rate in Sr containing glasses are related to the increase of free volume and the non-local effect that weakens the Si-O network.[27,28] Tilocca et al. investigated the structure of three phosphosilicate glasses (contain 45, 55, and 65 wt % SiO_2, respectively) by classic MD simulation using a shell-model potential. A possible correlation between the loss of bioactivity and the formation of inhomogeneous regions (aggregation between Ca^{2+} and PO_4^{3-} ions) was found based on their calculation results.[29] The development of ReaxFF reactive force field by van Duin et al. makes it possible for modelling the sol-gel synthesis of BG with a relatively low computational cost.[30] Côté et al. used reactive MD simulations to model the initial stages of sol-gel synthesis of BG. They found that compared to Ca-free system, the condensation rate is much faster when Ca is present in the initial solution.[31]

Although MD simulations have been widely applied to study BG, previous researches are mostly focused on silicate based bioactive glasses and very few studies were done on borate containing bioactive glasses.[32] Lacking of boron related potential parameters is one of the main reasons of limited MD simulations study of boroslicate and boron-based BG. Recently, we have developed potential parameters of boron oxide and successfully applied to the study of structure and properties of borosilicate and boroaluminosilicate glass systems.[32–34]

In this study, a series of B_2O_3/SiO_2 substituted Sr containing 55S4.3 BG ($56.5SiO_2$-$19.4Na_2O$-$16.5CaO$-$5.0SrO$-$2.6P_2O_5$, in mol%) were investigated by combining experimental studies and MD simulations. As compared to 45S5 BG, 55S4.3 BG with higher silica concentration is still bioactive but exhibits improved mechanical properties and chemical

durability, which is desired for some applications such bioactive coating on metal implants.[35] The addition of SrO in the glass composition was due to the ability of released Sr^{2+} ions to facilitate growth of osteoblast cells and inhibit osteoclast cells hence beneficial to bone growth.[27,28] These glasses were synthesized using the melt and quench process, their structures were characterized using Raman spectroscopy, and their properties such as density and in vitro bioactivity were determined and reported together with some initial simulation results of glass structure.[32] Our previous work (Ref 29) presented a combined experimental and simulation study of the system but only limited analyses of the glass structure from simulations were performed. In addition, dynamics properties such as ionic diffusion behavior and vibrational properties were calculated to understand the structure and bioactivity, glass property relations. The purpose of this paper is to provide a comprehensive report of MD simulations of this series of glasses with detailed short and medium range structure features as a function of B_2O_3/SiO_2 substitution. Furthermore, dynamic properties such as ionic diffusion behaviors and vibration results of these glasses were studied and the results were used to explain experimental data such as glass transition temperature (T_g) and in vitro bioactivity.

2. Methodology

2.1 MD simulation details

MD calculations were performed with the DL_POLY code [36], using a set of effective partial charge pairwise potentials in the Buckingham form with newly developed parameter for boron.[32] Details of the functional form, atomic charge and composition dependent boron potential parameters can be found in Ref [32]. Long-range Coulombic energies were calculated using the Ewald summation method with a precision of 10^{-6}. Integration of equation of motion was performed using the Velocity Verlet method with a time step of 1 femto-second (fs). Compositions of the glasses studied are shown in Table 1, where 0B denotes the composition of 55S4.3_5Sr and samples with silica was gradually replaced (25, 50, 75 and 100 mol%) with boron oxide were denoted as 25B, 50B, 75B, 100B respectively. To generate bulk glass structures, a simulated melt and quench process was adopted. A cubic simulation cell with system size of around 6,000 atoms and cell parameter of 41-43 Angstrom (Å) were used under periodic boundary conditions. The random generated initial structures with experimental density (Table 1) were energy minimized at 0 K and then relaxed at 300 K. The glasses were formed

from the simulated melt-and-quench process, where the systems were first melted at 6000 K for 60,000 steps (60 pico-second (ps)), relaxed at 5000 K for 100,000 steps (100 ps) and then cooled down to 300 K with a cooling rate of 5 K/ps. This cooling rate is much higher than experimental cooling rate but is commonly used in glass formation in MD simulations of oxide glasses, which is due to a compromise of realistic simulation time and reasonable generated glass structures. Recent studies have investigated the cooling rate effect on glass structure and various properties from MD simulations and found that many structural features and properties converge at a cooling rate much higher than the experimental values.[37–40] Tilocca investigated the effect of cooling rate and system size on the medium-range structure of 45S5 Bioglass with MD simulation and concluded that much lower cooling rate (less than 5-10 K/ps) was not necessary to obtain a reliable medium-range structure of multicomponent glasses.[39] Constant volume and temperature (NVT) ensemble was applied for all these steps. After melt and quench, the glass structures were further relaxed at 300 K using isothermal-isobaric (NPT) ensemble at ambient pressure (60 ps) and then a constant volume and total energy (NVE) ensemble for 60,000 steps (60 ps). Fig.1 shows a snapshot of glass structure of sample 25B generated from MD simulaiton. Final 40,000 steps under NVE ensemble at 300 K were recorded every 50 steps for structural analysis such as oxygen speciation, Q_n distribution, and pair distribution function (PDF). Polyhedral connection distribution and ring size distribution were calculated based on the last one configuration of NVE ensemble at 300 K. Glass transition temperature (T_g) from simulations was determined by plotting the total internal energy as a function of temperature during the cooling process. A change of slope of the energy was used as an indication of glass transition temperature and was determined by the intersection of tangents of energy curve in the glass and super cooled liquid ranges.[27,41]

To calculate diffusion coefficient and diffusion energy barrier, final glass structures were taken as an input for NVT and then NVE runs sequentially at the following temperatures: 1040, 1140, 1240, 1340, 1450, 1750, 2000, 2500, 2700, 3000, 3300, 3700 K for 1 ns (1,000,000 steps) at each temperature. The last 900,000 steps (900 ps) of NVE trajectories were recorded every 10 steps at each temperature to calculate the mean square displacement (MSD). MSD is defined as the distance ion travels over a time interval t averaged overall ions of the same type, that is:

$$< r^2(t) > = \frac{1}{n} \langle \sum_{i=1}^{n} |r_i(t) - r_i(t_0)|^2 \rangle \tag{1}$$

At long enough times, MSD exhibits a linear relationship versus time and ionic diffusion coefficients (D) were quantitatively extracted from the linear regime of the MSD curve via the Einstein equation:

$$D = \frac{1}{6} \lim_{t \to \infty} \frac{< r^2 >}{t} \tag{2}$$

where $< r^2 >$ is the mean square displacement and t is the time. To ensure statistical meaningful results, MSD calculations are usually averaged over the same type particles and over large number of origins. Based on Arrhenius relationship of diffusion coefficient, we know that:

$$D = D_0 \exp(-E_a/RT) \tag{3}$$

where E_a is the diffusion energy barrier, T is the temperature in kelvin, R is the gas constant. Take the logarithm on both sides of the equation (3), it is obtained:

$$\ln D = \ln D_0 - \frac{E_a}{RT} \tag{4}$$

Therefore, the activation energy can be calculated from the slope of the linear fitting of $\ln D$ relative to $1/T$.

Vibrational property was also studied with the help of MD simulation. Velocity auto-correlation function (VACF) is defined as $c(t) = \langle v(t) \cdot v(0) \rangle$ [42], in which $v(t)$ and $v(0)$ are the velocity at time t and time 0 respectively. Partial and total vibrational density of states (VDOS) can be obtained through Fourier transformation of the VACFs:

$$f(\omega) = \frac{2}{\pi} \int_0^{\infty} C(t) \cos(\omega t) dt \tag{5}$$

where ω is vibration frequency, $c(t)$ is velocity autocorrelation function.

Three samples were prepared for each glass composition from MD simulations with the same cooling procedure but different initial configurations with atoms randomly placed in the simulation cell. The structure and dynamic properties reported were averaged over the three parallel samples.

2.2 Experimental details

The glasses were prepared by thoroughly mixing analytical grade H_3BO_3, $NH_4H_2PO_4$, SiO_2, $NaCO_3$, $CaCO_3$ and $SrCO_3$ chemicals (30 g of total raw materials for each batch) before degassing in an Al_2O_3 crucible at 850 °C for 1 h and melting at 1450 °C for 1 h in an electrical furnace. Molten glasses were poured onto a stainless plate and cooled to room temperature. High- resolution X-ray diffraction (XRD) was used to confirm the non-crystalline structure of glass (7.5% of sodium calcium phosphate ($Na_3Ca_6(PO_4)_5$)-crystallized phase was found in sample 25B). Density measurements were taken on the glass powders using the specific gravity method with density bottles at room temperature. Detailed experimental procedure for glass synthesis, physical property measurements and in vitro bioactivity studies have been reported in the previous paper.[32] Additionally, thermal analyses of these glasses were performed using differential scanning calorimetry (DSC), which was carried on a NETZSCH STA 499 F3 in an argon environment with a gas flow of 60 mL/min, a heating rate of 20 ˚C/min, with a powdered glass sample (particle size between 32 μm to 45 μm) weighing between 22 mg and 25 mg in an Al_2O_3 pan without a lid. The glass transition temperatures (T_g) were determined by commonly adopted intersection of tangents at the onset of glass transition where heat capacity changes based on the measured DSC curves with an estimated error of $\pm$ 3 °C.[43] It is worth noting that T_g measured from DSC depends on the heating (or cooling) rate while other parameters such as particle sizes of sample can also have an effect.
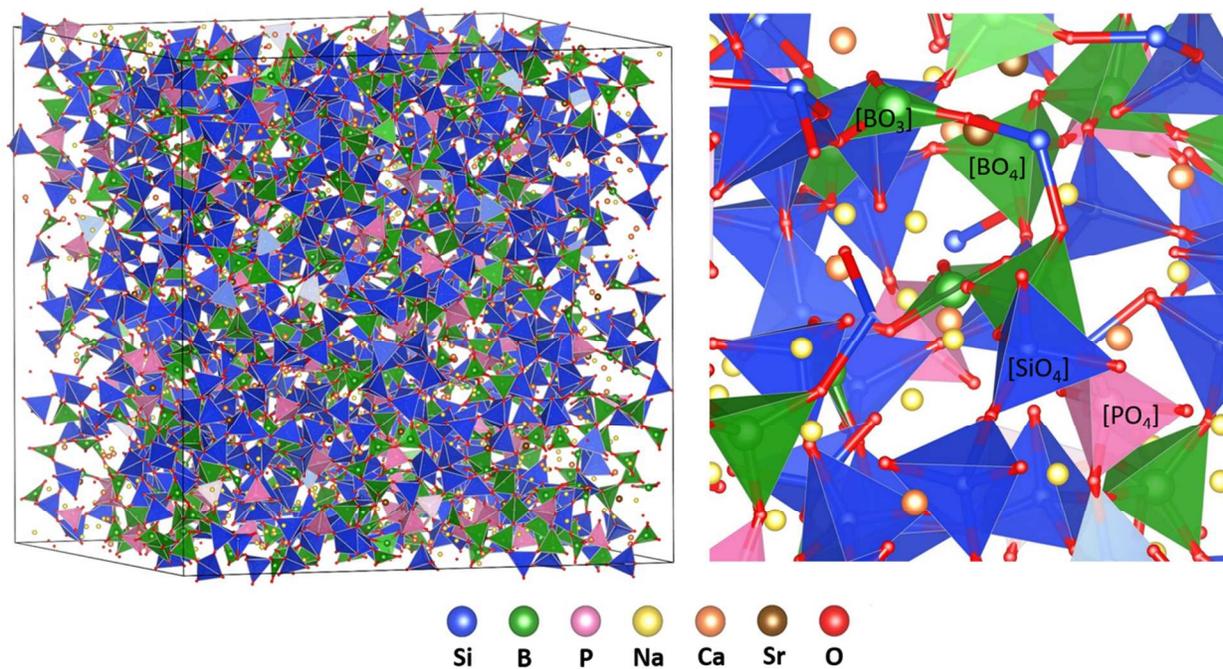
Fig. 1 Whole bulk (left) and zoomed-in (right) final configurations of sample 25B.

3. Results

Table 1 Batched glass compositions; experimental glass density (ρ) and T_g; atom number used in MD simulation.

Sample	B_2O_3	SiO_2	Na_2O	CaO	SrO	P_2O_5	Exp. ρ (g/cm^3)	Exp. T_g (˚C)	Ref. T_g (˚C)	MD T_g (˚C)	Atom number used in MD simulation						
			(mol%)								B	Si	Na	Ca	Sr	P	O
0B	0	56.5	19.4	32.2	5.0	2.6	2.78 ± 0.03	550	580[a], ~561[b], ~540[c]	1245	0	1173	806	343	104	108	3466
25B	14.1	42.4	19.4	31.3	5.0	2.6	2.68 ± 0.03	540		1053	534	802	734	312	95	98	3424
50B	28.2	28.3	19.4	30.3	5.0	2.6	2.62 ± 0.03	538		880	980	492	674	287	87	90	3390
75B	42.3	14.2	19.4	29.4	5.0	2.6	2.55 ± 0.04	496		784	1359	228	623	265	80	84	3361
100B	56.5	0	19.4	28.6	5.0	2.6	2.50 ± 0.01	480		627	1687	0	579	246	75	78	3336

a 55S4 analyzed using DSC with a heating rate of 10 ˚C/min.[44]

b S53P4 analyzed using differential thermal analysis (DTA) with a heating rate of 15 ˚C/min and weight of 60 mg in platinum pans under N_2 atmosphere. [45]

c 5 mol% CaO substituted with SrO in S53P4 analyzed using DTA with a heating rate of 30 ˚C/min and weight of 50 mg in platinum pans under N_2 atmosphere. [46]
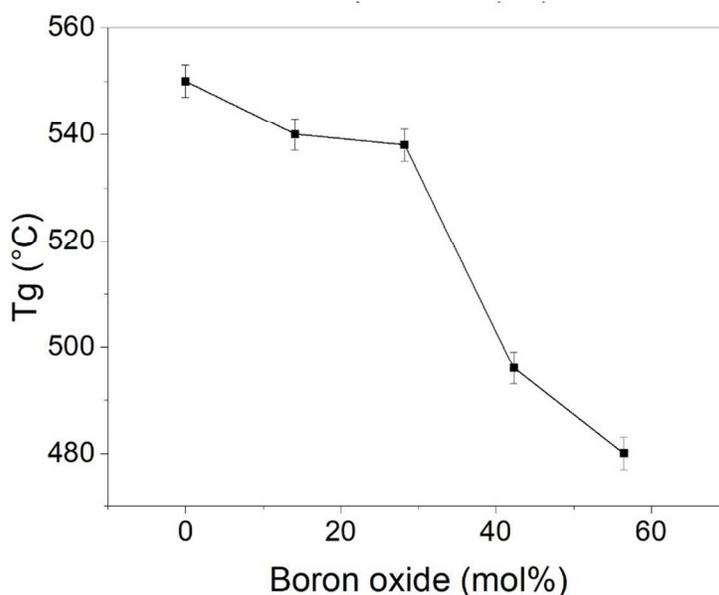
Fig. 2 Experimental T_g for different glass samples determined from DSC

Experimental determined T_g for different glass samples was shown in Fig.2 and Table *1*, together with those from literature for the 0B composition (Table *1*). It can be seen that B_2O_3/SiO_2 substitution leads to a decrease of T_g as the increase of B_2O_3 content. It was also found in literature that addition of B_2O_3 reduced the T_g of 45S5 (up to 4 mol% B_2O_3)[47] and a Si-Ca-P glass system.[48] T_g of 0B is ~550 ˚C measured with DSC, which is generally agree with literature data (~540 ˚C)[46] with a slightly variation due to different heating rate used. T_g also can be determined from MD simulation based on the change of slope of potential or configuration energy vs. temperature. As can be seen in Table *1*, in general, T_g from MD has a higher value than that from experiments. For example, the T_g from MD is 1245 °C for 0B and 627 °C for 100B. However, the trend of T_g with composition: decrease of T_g with increase of B_2O_3, is consistent with experiment. The higher T_g from MD simulations is mainly due to the much higher cooling rate used in MD simulations than in experiments. It has been recently shown in MD simulations of sodium borosilicate glasses that slower cooling rate leads to a decrease of glass transition temperature.[37] When extrapolated to experimental cooling rate, the simulated glass transition temperature is in similar ranges of those from experiments. Thus here it is more important to compare the change of T_g as a function of composition than the absolute value. It

has been shown both experimental value and MD shown similar trend of T_g with glass composition (Table 1).
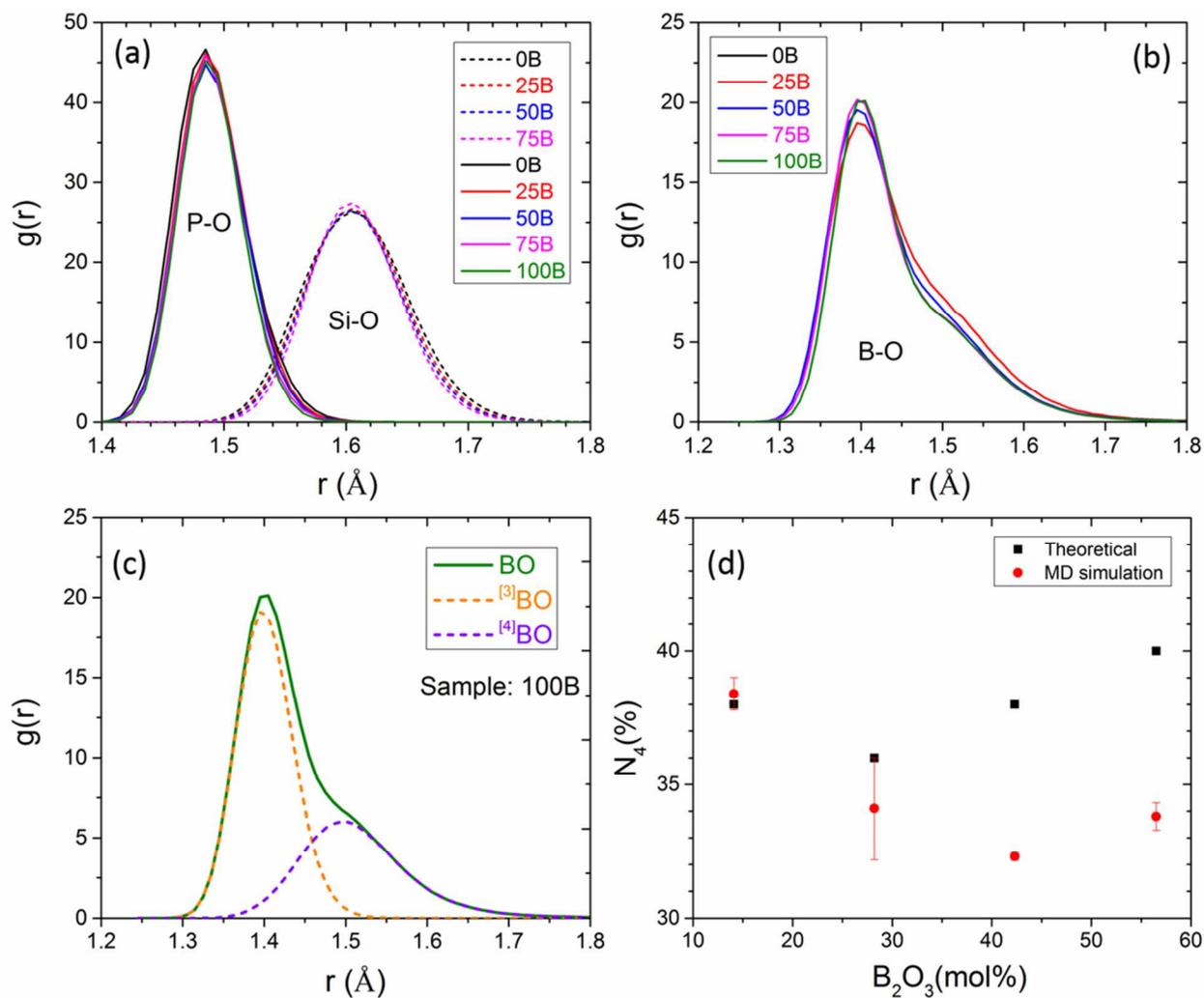
Fig. 3 Pair distribution function (PDF) for (a) P-O (solid line) and Si-O (dash line) (b) B-O in different bioactive glasses; (c) Decomposed PDF of B-O bond in 100B Sample; (d) Fraction of four-fold boron (N_4) distribution: a comparison between MD simulation results and theoretical values.
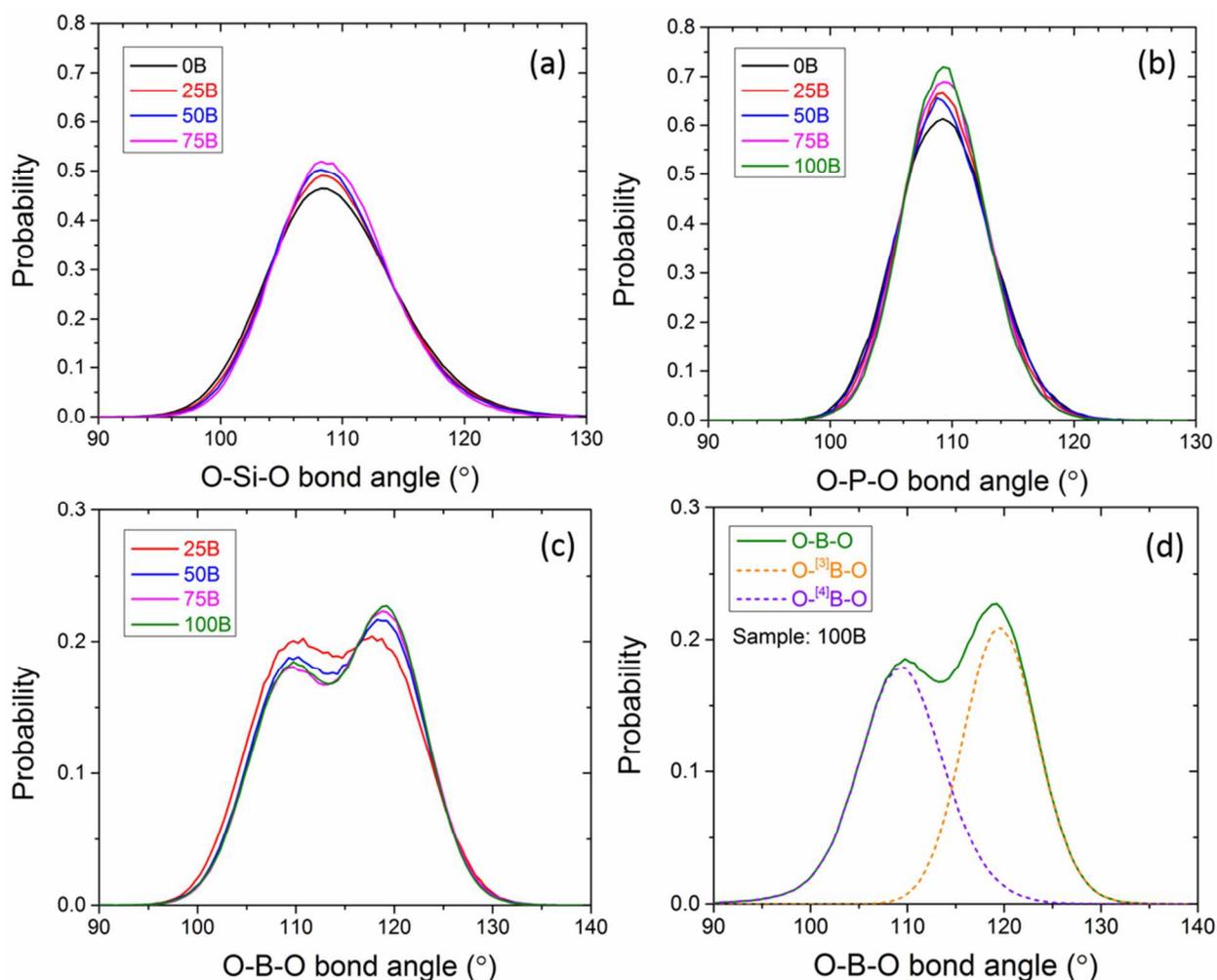
Fig. 4 Bond angle distribution (BAD) for (a) O-Si-O (b) O-P-O (c) O-B-O in different bioactive glasses (d) Decomposed BAD of O-B-O angle in 100B Sample

Pair distribution function (PDF) is a probability density function commonly used for material structure analysis. The first peak position gives the nearest neighbor distance between two corresponding atoms. As shown in Fig. 3(a), the bond lengths of Si-O and P-O were determined to be 1.61 Å and 1.49 Å, respectively. Two peaks were observed in the B-O PDF (Fig. 3b and c), corresponding to [3]B-O (~1.4 Å) and [4]B-O (~1.5 Å), respectively. The fraction of four-coordinated boron (N_4) is an important structure parameter for boron-containing glass. As shown in Fig. 3(d), the N_4 data derived from MD simulation shared similar variation trend with theoretical values[32] and the difference was within 7%. Bond angle distribution (BAD) was analyzed for the angle inside a polyhedron. Both of O-Si-O and O-P-O has a peak location around 109° (Fig. 4a and b). As compared to O-P-O, O-Si-O has a wider distribution. Two main

peaks in the BAD plots of O-B-O (Fig. 4c and d) were observed: one located at around 109.5° corresponding to the four-fold coordinated boron ([4]B) and the second peak around 120° corresponding to the three-fold coordinated boron ([3]B).
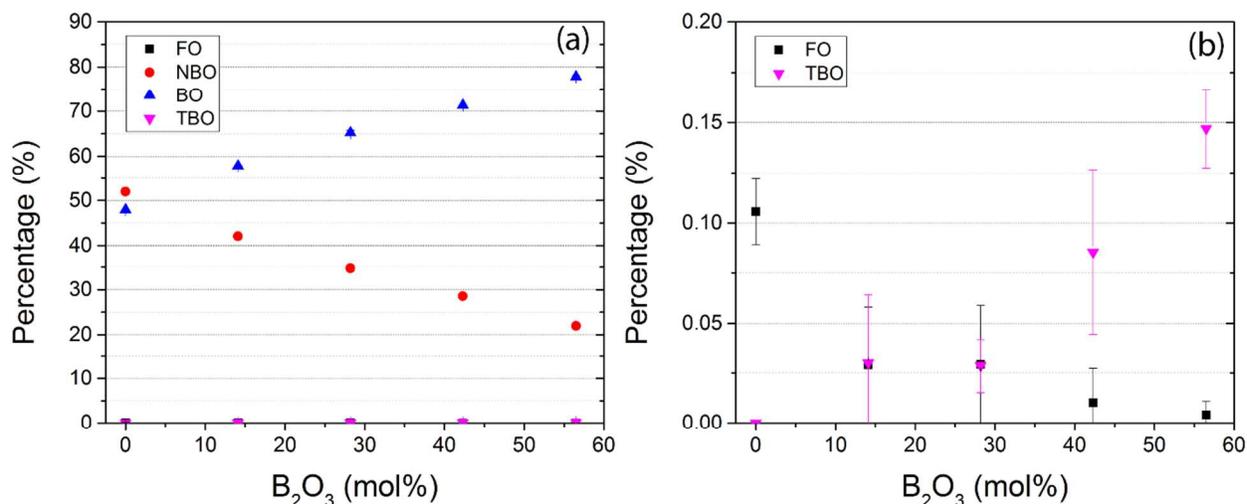
Fig. 5 Oxygen species distribution for the bioactive glasses from MD simulations: (a) all species (b) low percentage part that contains data for FO and TBO only. (three parallel tests were used to get the standard deviation)

For the oxygen species analysis, the fraction of three-bonded oxygen (TBO), bridging oxygen (BO), non-bridging oxygen (NBO) and free oxygen (FO), which defined as oxygen atom connected to three, two, one and none glass forming cation (Si, B and P) respectively, have been calculated for each glass composition. As can be seen from Fig. 5b, FO and TBO are tiny minorities with no more than 0.2 % in all these glasses. With the increase of B_2O_3 concentration, NBO was converted to BO, leading to a near linear increase of BO percentage (Fig. 5a). The conversion of NBO to BO was not surprise since when 1 mole of SiO_2 was substituted by B_2O_3, the mole ratio of (Si+B)/O would increase.
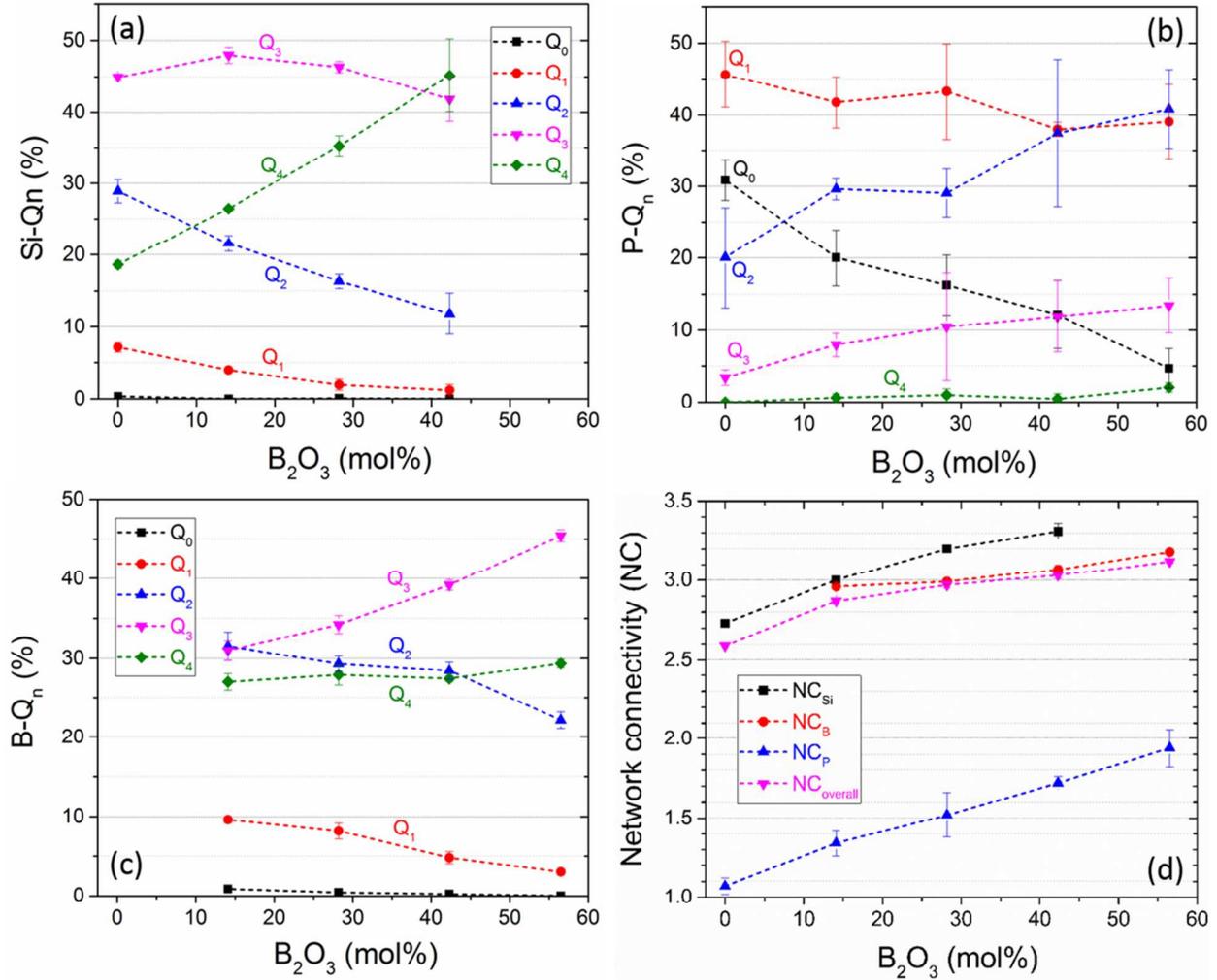
Fig. 6(a) Si-Q_n distribution (b) P-Q_n distribution (c) B-Q_n distribution (d) Glass network connectivity (NC) of the bioactive glasses from MD simulations (three parallel tests were used to get the standard deviation)

Considering there are two main kind of oxygen species (BO and NBO) in the glass structure, we can use Q_n to differentiate various polyhedrons, where "n" stands for the number of surrounding BO atoms connected to each center glass-former atom (Si/B/P). With Q_n distribution data, glass network connectivity (NC_X, X=Si, B, P) of each glass former atom X can be determined by $NC_X = \sum_{n=0}^{4} n \times Q_n^X$. The overall NC is further calculated by $NC_{overall} = \frac{NC_{Si} \times [SiO_2] + NC_B \times 2 \times [B_2O_3] + NC_P \times 2 \times [P_2O_5]}{[SiO_2] + 2 \times [B_2O_3] + 2 \times [P_2O_5]}$, where $[SiO_2]$, $[B_2O_3]$ and $[P_2O_5]$ are the mol% of SiO_2, B_2O_3, and P_2O_5 in glass composition, respectively.

16

From Fig. 6(a,c) it can be seen that Q_1 and Q_2 around both Si and B are decreased as the increase of B_2O_3 content, while the increase of Q_4 is dominated for Si, and for B the increase of Q_3 is dominated. Such change of Q_n distribution around Si and B resulted the increase of NC_{Si} and NC_B as the increase of B_2O_3. For P (Fig. 6b), the basic trend is the decrease of Q_1, Q_0 and increase of Q_2, Q_3 species, also leading to the increase of NC_P (Fig. 6d). We further noticed that the standard deviations for P-Q_n distribution (Fig. 6b) are much higher than that for Si-Q_n and B-Q_n (Fig. 6a and Fig. 6c). This should related to the relatively small mole percentage of P_2O_5 in glass compositions. On the other hand, this may indicates that the Q_n distribution around P was not as stable as that for B and Si.
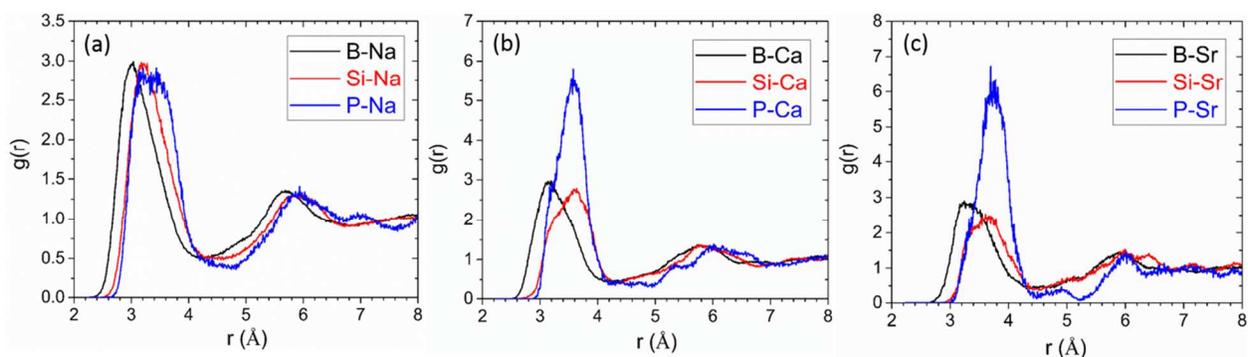
Fig. 7 Pair distribution function (PDF) for sample 50B (a) B/Si/P-Na (b) B/Si/P-Ca (c) B/Si/P-Sr calculated from MD simulations.

One of the glass samples (50B) was used here as a representative for the glass former-modifier PDF calculation (Fig. 7). The intensity of peak indicates the probability (excluded the effect of atom concentration) to find corresponding atom pairs. In general, the distances between B and glass modifiers (Na/Ca/Sr) were lower than corresponding values for Si and P, indicating smaller average bond distances between boron and nearest modifiers. Based on similar peak intensity for B/Si/P-Na shown in Fig. 7a, we can inference that Na tend to distributed evenly around B. Si and P. If we further compare the peak intensity of P-Na, P-Ca and P-Sr, it can be seen that the first peak intensity for P-Ca/Sr (Fig. 7b,c) is about twice as that for P-Na (Fig. 7a). In addition, the peak intensity for P-Ca and P-Sr are also higher than that for B/Si-Ca/Sr. These results indicated within the first nearest neighbor shell, Ca and Sr tend to more gather around P to create NBO, which is in agreement with the fact that NC_P is lower than NC_{Si} and NC_B (Fig. 6d).
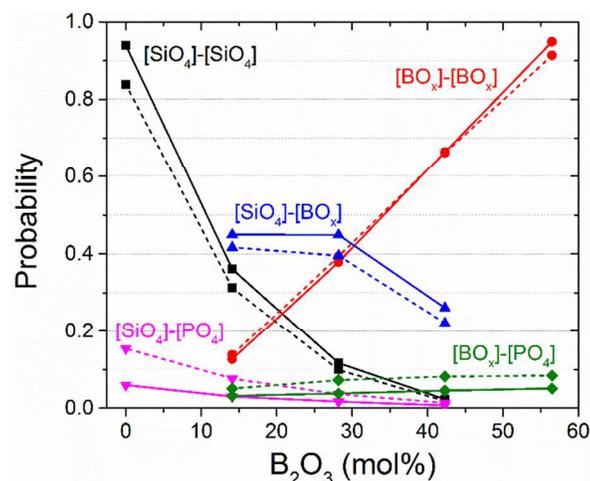
Fig. 8 polyhedral connection distribution for different glasses (points on solid line are MD simulation results, points on dash line are calculated based on a random distribution assumption)

Fig. *8* shows the polyhedral connection distribution for glass samples with different B_2O_3 concentration. The only missing possible connection is $[PO_4]$-$[PO_4]$. Because based on our MD simulation results, there is barely any $[PO_4]$-$[PO_4]$ connections (no more than 3 for each glass compositions). We also calculates the connection probability (the dash line shown in Fig. *8*) by assuming a random distribution of glass network former atoms.[34] Comparing the MD simulation derived polyhedral connection distribution (solid line) with the predictions of a random network distribution (dash line), we found the connection probability $[SiO_4]$-$[PO_4]$ and $[BO_x]$-$[PO_4]$ calculated from MD simulation are lower than the predictions of a random network distribution, which should related to the fact that $[PO_4]$ groups tend to be isolated. On the contrary, the higher connection probability of $[SiO_4]$-$[SiO_4]$ and $[SiO_4]$-$[BO_x]$ as compared with random network distribution data indicated Si^{4+} and B^{3+} are strong glass network formers and tend to mixed with each other and form the glass network structure together.

18
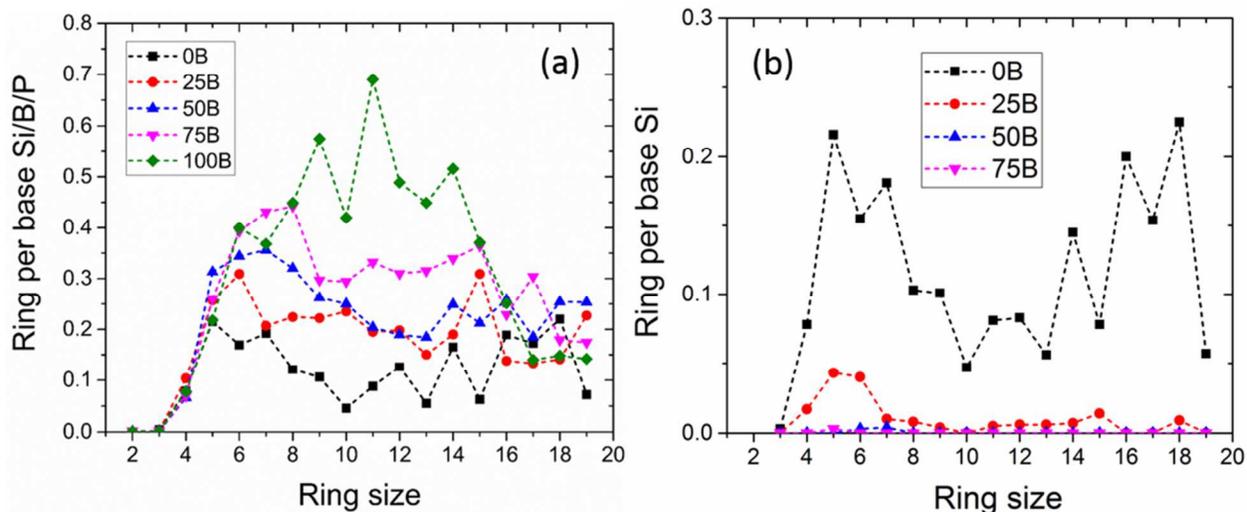
Fig. 9 Primitive ring size distribution of bioactive glasses from MD simulations: (a) considering Si, B and P as glass network formers (b) considering Si as glass network former only

Ring size distribution is another important method of characterizing the medium range structure of glass network. Glass former polyhedral can connected with each other by corner-sharing to form rings of different size. A ring will be primitive if it contains the minimum number of examined network formers.[49] For pure silica glass, the ring size distribution shows a symmetric Gaussian type distribution with a peak at around six.[50] Incorporation of glass network modifiers such as Na_2O into silica glass will depolymerize the Si-O network, leading to a decrease of ring around six and an increase of larger rings. Fig. 9(a) shows primitive ring size distribution by considering Si, B and P all together as glass network formers. Due to the high concentration of glass modifiers (40.9 mol%), all the calculated ring sizes shown a wide distribution range. It also can be seen that adding boron in to silicate glass leads to an obvious increase of ring size of 6~15. If we only consider Si as glass former, the corresponding ring size distributions are shown in Fig. 9(b). Under this circumstances, sample 25B has a peak position around 6, and there is barely any ring exist for samples (50B and 75B) with higher B_2O_3 concentration.
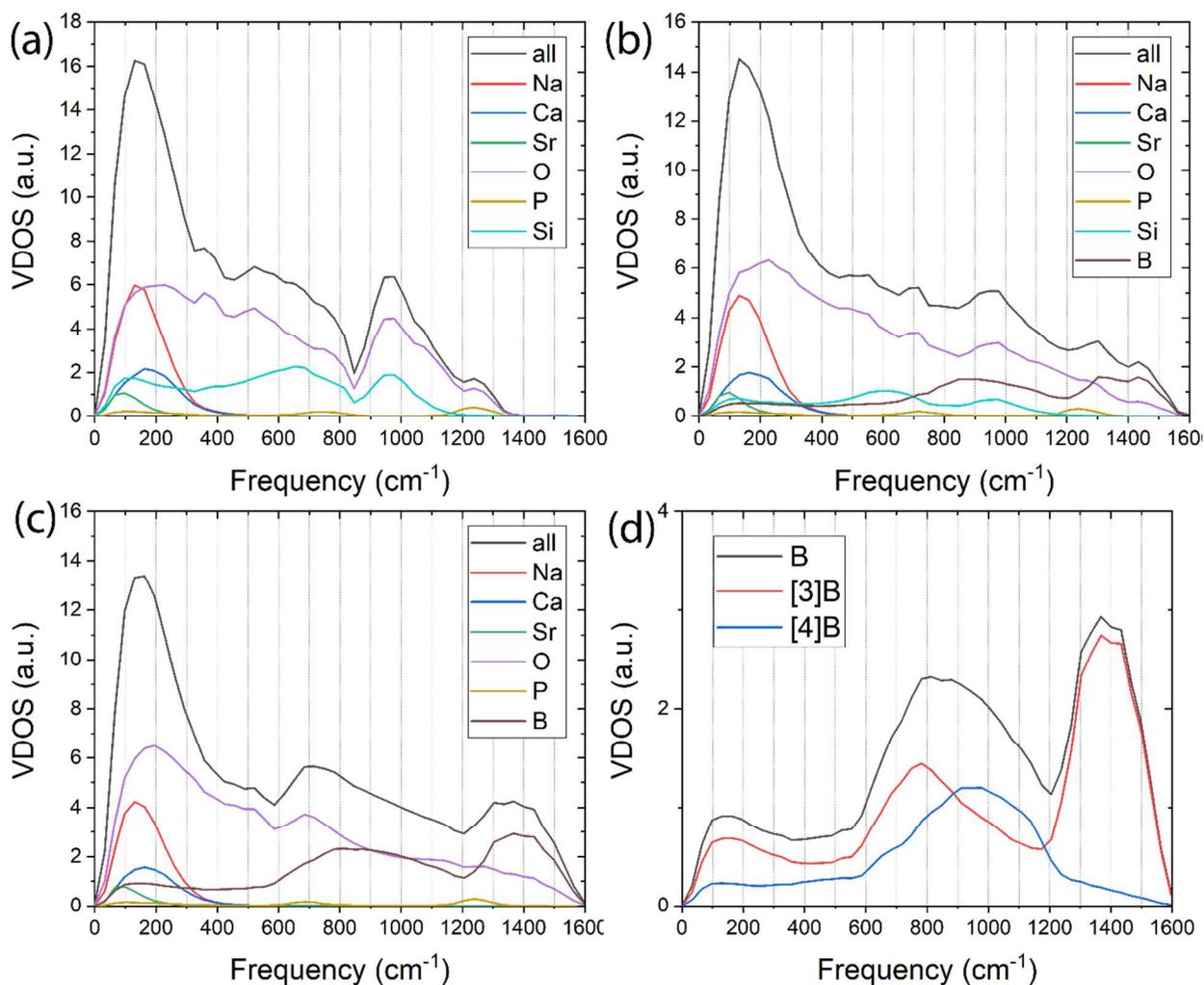
Fig. 10 Total and partial vibrational density of states (VDOS) for different glass samples at 300 K: (a) 0B (b) 50B (c) 100B (d) Partial VDOS for [3]B and [4]B in sample 100B

Vibrational properties of the glasses were calculated from velocity autocorrelation functions. Velocity density of states (VDOS) of three representative samples (0B, 50B and 100B) at 300 K are shown in Fig. 10. VDOS shown in Fig. 10a for sample 0B (55S4.3_5Sr) is quite similar to pervious reported MD simulation results of VDOS for 45S5.[27] For all the samples, the first peak has same location at around 150 cm^{-1}. This strongest peak consisted contributions from all the ions and modifier ions (Na, Ca and Sr) have no contribution to higher frequency vibration features. For sample 0B, the second strong peak was around 950 cm^{-1}, which can be assigned to Si-O stretching vibrations.[27] For B_2O_3/SiO_2-subtibuted samples (50B and 100B), the VDOS at the high frequency shown some variation due to the contribution from boron. Pedesseau et al.[51]

calculated the VDOS for a borosilicate glass by first-principles MD simulations. It is reported that [3]B gives rise to a pronounced peak at around 680[-1] cm and a broad band between 1100-1500 cm^{-1}, and the [4]B vibrational modes are mainly located between 800-1200 cm^{-1}. [51] As shown in Fig. 10d, the partial VDOS for [3]B and [4]B generally well agreed with the above mentioned first-principles calculation results.
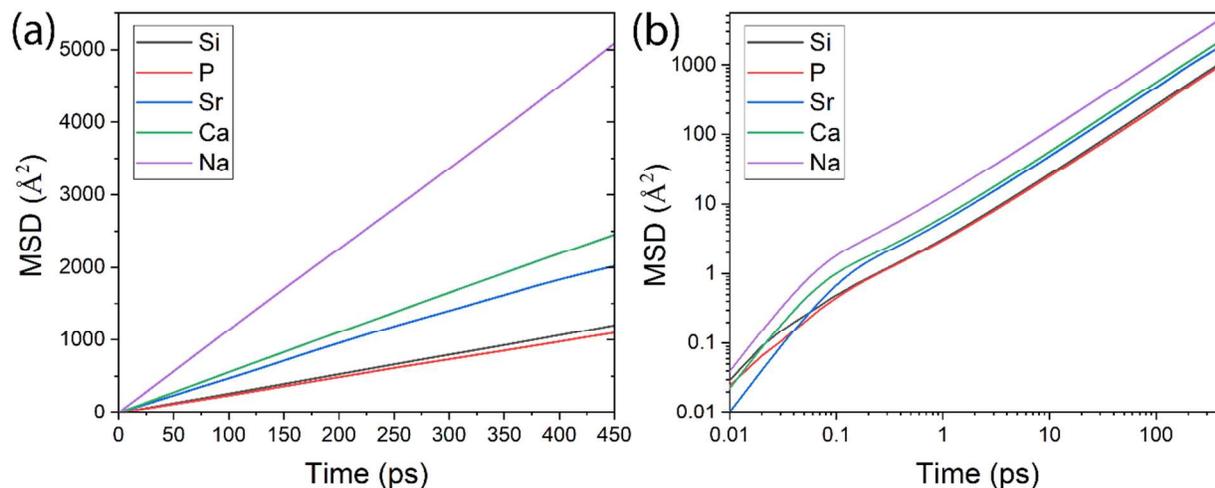
Fig. 11 MSD for all the ions in sample 50B at 3700 K: (a) linear scale (b) logarithm scale
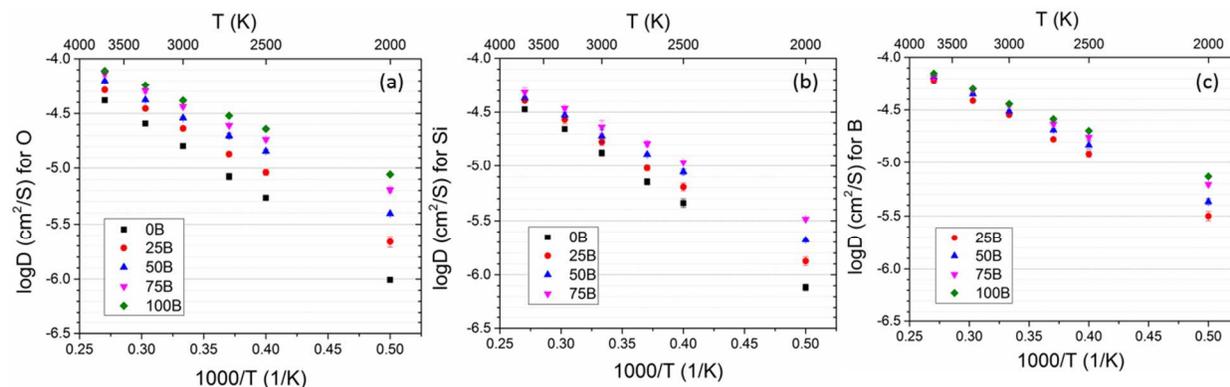
Fig. 12 High temperature range (2000-3700 K) diffusion coefficients for (a) O (b) Si (c) B calculated from MD simulations (three parallel tests were used to get the standard deviation)

21
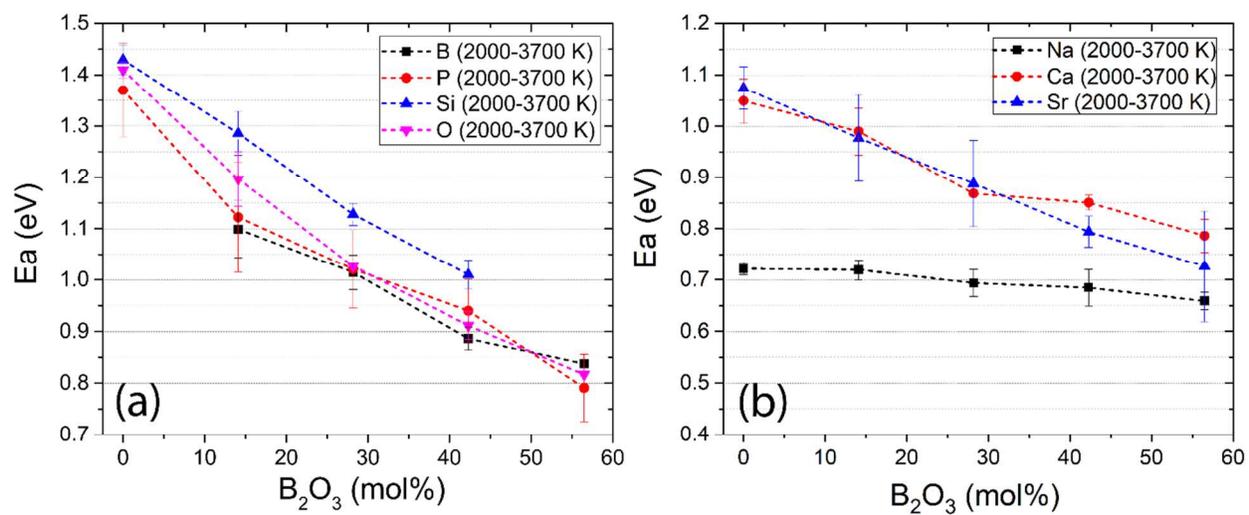
Fig. 13 High temperature range (2000-3700 K) diffusion energy barriers for (a) glass formers (b) glass modifiers (three parallel tests were used to get the standard deviation).
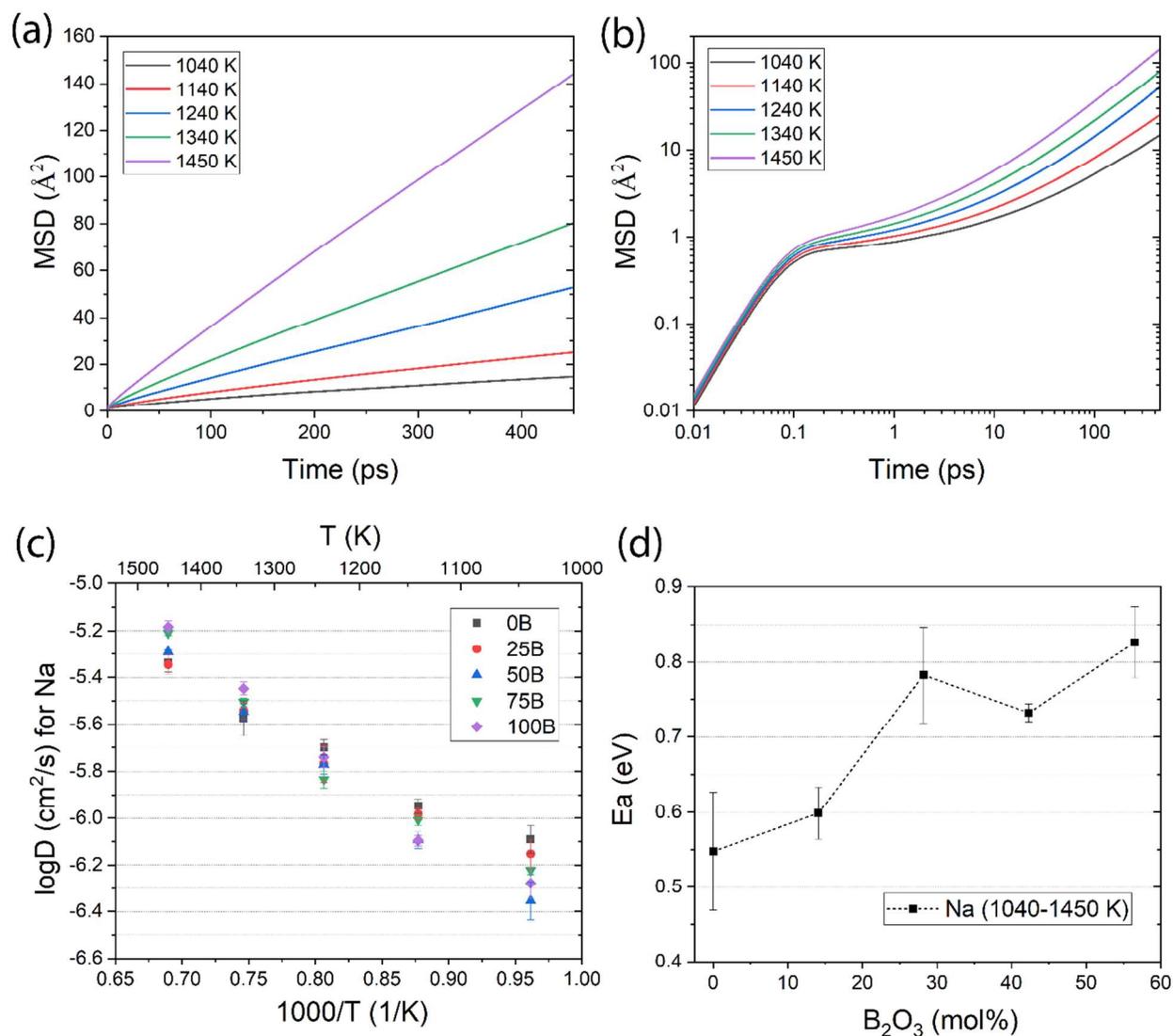
Fig. 14 Low temperature range (1040-1450 K) (a) MSD versus time linear scale (b) MSD versus time in logarithm scale (c) Arrhenius plot of diffusion coefficients (lnD) versus 1000/T (d) diffusion energy barriers for Na (error bar from three parallel samples) as a function of B_2O_3 concentration (mol%)

Ion diffusion properties such as diffusion coefficient (D) and diffusion energy barrier (E_a) in glass and melts were derived from mean square displacement calculations at different temperatures. Fig. 11 shows the MSDs of all ions in sample 50B glass at 3700 K as a reference, where MSDs are proportional to t at longer time region.[41] The last 20 ps of the linear range of MSD versus time was used to calculate the diffusion coefficient based on Einstein's equation (Eq. 2). The calculation of diffusion energy barrier were derived from the Arrhenius plot Ln D vs 1/T around T_g. Two range behavior were observed where there is a slope change close to the glass

23

transition temperature. At high temperature range (2000-3700 K), the system is considered to be in liquid (or molten) state with all ions that are mobile. Fig. 12 shows the diffusion coefficients for glass former ions above T_g, which in the same order range with first-principle calculation results for sodium borosilicate glass melts. [52] From Fig. 13 (a,b) it can be clear seen that the increase of B_2O_3 lead to a decrease of E_a for all the ions at the high temperature range, consistent with the role of boron oxide decrease the melting temperature and viscosity of the melt. Such effect is more obvious for B, P, Si, O, whose E_a value drops from ~1.4 to ~ 0.8 eV. The significant decrease of E_a (especially for glass formers) at high temperature range well explained the experimental observed fact that adding certain amount B_2O_3 into silicate glass can decrease the melting point and increase the fluidity of glass melts. [53,54] In the low temperature range (1040-1450 K), Si, B and O are immobile due to their low diffusivity as backbone of the glass forming network. The MSDs and diffusion coefficient for Ca and Sr are reported in supplementary materials. As compared to Ca and Sr, Na has smaller ion radius and lower charge thus showing the highest diffusivity. The MSDs calculation for Na (Fig. 14a,b) based on the 1 ns trajectory was shown in Fig. 14c. The diffusion coefficients with associated error bars (error bars were obtained from 3 parallel samples with different initial configurations but the same thermal history) were also reported in V, while that for Ca ranges from 0.68 to 0.89 eV, depending on the composition for temperatures 1000-1400K, similar to our low temperature range.[55] As Na ions diffusion plays a key role in the ion exchange in the initial stage of the bioactivity mechanism, the increase of Na diffusion energy barrier with B_2O_3 concentration of the series of glass studied in this work suggests a decrease of bioactivity, which agrees well with experimental results. This also supports the effectiveness of dynamic descriptor on bioactivity, in addition to the commonly used structural descriptor.[55]

Table *2* and these values are comparable to other MD simulation results. [27,55,56] On the experimental side, it is reported that tracer diffusivity of [22]Na in $0.2Na_2O-0.8B_2O_3$ glass increased from ~10^{-13} cm^2/s to ~ 10^{-11} cm^2/s as the temperature increased from ~500 K to ~600 K.[57] Sodium tracer diffusion coefficients measured in $(CaO-Al_2O_3)_x(2SiO_2)_{1-x}$ glasses at 800 °C decreased from ~$10^{-7.5}$ cm^2/s to ~ $10^{-12.5}$ cm^2/s as the x value increased from 0.175 to 0.9.[58] Diffusion energy barriers for Na, Ca and Sr for the low temperature ranges are reported in Table 3. Na diffusion energy barriers range from 0.55 to 0.83 eV, increases with B_2O_3 concentration

(Fig. 14d), which can be explained by the increase of glass network connectivity with B_2O_3. Wu et al.[59] measured the sodium tracer diffusion coefficients in $(Na_2O)_{0.2}(B_2O_3)_y(SiO_2)_{0.8-y}$ for temperatures up to ~350 °C and found that the activation enthalpy increases with increasing values of y from 0.73 eV to 1.05 eV, which is in agreement with the E_a variation trends for Na at low temperature range. The activation energy derived from electrical conductivity measurement for $53.5SiO_2$-$26.1B_2O_3$-$20.4Na_2O$ glass is 0.78 eV.[60] Murugavel et al. measured the DC conductivity of alkali ions in 45S5, 55S4.3 and 60S3.8 glasses.[61] The energy barrier for 45S5 was reported to be 0.96 eV and the energy barrier for 55S4.3 should be higher than that for 45S5. [61] Previous MD simulation of 45S5 bioglass shown that the E_a for Na ions were around 0.56 eV, [24] which agrees well with to the 0B value of 0.53 eV in this study. Tilloca studied the Na, Ca and F ion diffusion in fluorine containing bioactive glasses using MD simulations and found that diffusion coefficients can be a dynamic descriptor of bioactivity of glasses.[55] For the two composition studied, Na diffusion energy barrier ranges 0.36 to 0.75 eV, while that for Ca ranges from 0.68 to 0.89 eV, depending on the composition for temperatures 1000-1400K, similar to our low temperature range.[55] As Na ions diffusion plays a key role in the ion exchange in the initial stage of the bioactivity mechanism, the increase of Na diffusion energy barrier with B_2O_3 concentration of the series of glass studied in this work suggests a decrease of bioactivity, which agrees well with experimental results. This also supports the effectiveness of dynamic descriptor on bioactivity, in addition to the commonly used structural descriptor.[55]

Table 2 Diffusion coeffcients (10^{-6} cm^2/s) of Na in low temperature range

T (K)	0B	25B	50B	75B	100B
1040	0.82 ± 0.11	0.71 ± 0.10	0.45 ± 0.08	0.60 ± 0.03	0.53 ± 0.08
1140	1.13 ± 0.08	1.04 ± 0.06	0.81 ± 0.07	0.98 ± 0.05	0.80 ± 0.04
1240	2.00 ± 0.15	1.72 ± 0.30	1.70 ± 0.16	1.47 ± 0.13	1.82 ± 0.18
1340	2.69 ± 0.48	2.88 ± 0.21	2.84 ± 0.24	3.13 ± 0.12	3.58 ± 0.23
1450	4.62 ± 0.43	4.53 ± 0.41	5.13 ± 0.09	6.18 ± 0.16	6.56 ± 0.40

Table 3 Diffusion energy barrier (eV) for Na, Ca and of Sr in low temoperature range

Ion	0B	25B	50B	75B	100B

25

Na	0.55 ± 0.08	0.60 ± 0.03	0.78 ± 0.06	0.73 ± 0.01	0.83 ± 0.05
Ca	0.65 ± 0.09	0.64 ± 0.08	1.04 ± 0.05	0.93 ± 0.06	1.06 ± 0.07
Sr	0.70 ± 0.19	0.64 ± 0.14	0.94 ± 0.11	0.96 ± 0.13	1.17 ± 0.14

4. Discussion

According to experimental DSC results, T_g is decreased as the increase of boron oxide concentration. It is known that T_g is related to the viscosity since one of the definition of T_g is -- the temperature at which the shear viscosity is equal to a fixed value (usually taken as 10^{12} Pa s)[62]. Viscosity can be further related to diffusion coefficient. At higher temperature (> 1.2 T_g), diffusion coefficients are expected inversely proportional to the viscosity.[63] Thus the T_g of glass should be able to connected with ion diffusion coefficient. In MD simulation, self-diffusion coefficient can be simply calculated from MSD via the Einstein equation. Fig. 12 shows the diffusion coefficient (D) calculated for main glass formers (Si, B and O) in glass melts (2000 K — 3700 K) from MD simulation. It can be observed that for glasses contain both B_2O_3 and SiO_2 (25B, 50B and 75B), D of B is always higher than that of Si and O. Comparison between different samples indicated that as the increase of B_2O_3 content, diffusion coefficients for Si, B and O (Fig. 12a-c) increased, corresponding to a decrease of viscosity and thus in consistent with the changing trend of experimental determined T_g (decreased as the increase of B_2O_3 content, see Table 1).

Except for dynamic properties such as diffusion related data that mentioned before, with the help of MD simulation, the bulk structure of different glasses also can be quite well understood. Oxygen speciation and Q_n calculation well proved that substitution of Si with B leading to an increase of glass network connectivity (NC). Polyhedral connection and ring size distribution study shown that Si and B are tend to connected with each other together to form a 3D glass structure. But how to connect these microscopic structure features with macroscopic properties is always a great challenge. Based on previous MD simulation study for boron-free silicate glass, it

is expected that increase of chain-like fragments would increase the glass dissolution rate and thus increase the bioactivity.[64] There are also some experimental researches try to connected NC with bioactivity and it is well accepted that bioactive silicate glasses usually have NC between 2~3 and the bioactivity tend to decrease as the increase of NC.[65–67] In this work, the addition of boron oxide into the silicate glass makes things even more complicated. It is reported that for borosilicate glass, boron usually has much higher dissolution rate as compared to silicon.[68] So the connection between NC and bioactivity found in silicate glass may not work for borosilicate glass system. First-principle calculations of hydrolysis reaction barriers in sodium borosilicate glass shows that the energy barrier of breaking cation–oxygen–cation linkages by reaction with water decreased according to the following sequence: Si-O-Si > Si-O-B > B-O-B.[23] Based on the polyhedral connection distribution results (Fig. 8), we know that the connection probability of $[SiO_4]$-$[SiO_4]$ and $[SiO_4]$-$[BO_x]$ decreased as the increase of B_2O_3. Thus it is expected that the B_2O_3/SiO_2 substitution in 55S4.3 would result an increase of glass dissolution. We further calculated the ring size distribution without considering boron as a glass former. As shown in Fig. 9b, subtraction of boron leaves a much fragment structure: for sample with higher boron concentration (50B and 75B), there is almost no ring structure existed. In reality, how the borosilicate glass network would evolve with more and more boron released from the original structure is still not clear and could be studied in the future work with the help of MD simulation.

Bioactivity is another important consideration for this series glass and has been elaborated in our previous work [32] that address on the experimental results. The variation of pH value is a good indicator of bioactivity and it is well known that HAp tend to formed at higher pH ($> \sim 8$) values. Aza et.al [69] studied the influence of pH at the silica-based material/SBF interface on HAp formation. The results shown that all the bioactive materials show a rapid increase in pH (tend to reach pH > 9) at the material/SBF interface. A solubility diagram for various Ca phosphate minerals cited by the author as a proof shown that at SBF HPO_4^{2-} concentration (10^{-3} M), when pH = 9.5~10.5 the solution is supersaturated with respect to HAp and precipitation takes place. For silica-based bioactive glass, it is believed that the ionic exchange of H_3O^+ from SBF for Na^+, K^+, Ca^{2+}, etc. induces the formation of amorphous silica hydrogel layer and the increase in pH at the material/SBF interface. In our experimental study, although the pH at material/SBF interface was not determined, the overall pH variation of SBF with different glass samples can still provide some useful information. As found earlier, [32] the pH value of SBF for 0B sample

(without boron) increased significantly at the initial immersion stage and HAp fully covers the sample surface after 3 weeks of SBF treatment. While for the rest boron contend samples, pH values of SBF remains largely unchanged during 3 weeks immersion. Also, addition of boron oxide almost completely inhibits the HAp formation of the glasses in SBF solution. This can be explained by the fact that higher boron oxide content leads to higher dissolution rate hence release of more H_3BO_3 to the solution, due to its acidic nature, leading to a decrease of pH value. In this situation, the capability of formation of silica gel layer is reduced. Since silica gel is where the calcium ions and phosphate groups land and accumulate, missing the silica gel layer due to fast dissolution inhibits the formation of HAp, hence decreases the bioactivity of the glasses.

5. Conclusion

By using classical MD simulations with recently developed composition dependent boron potentials, the short and medium range glass structures and properties such as ion diffusion and glass transition temperatures of a series of B_2O_3/SiO_2 substituted SrO containing 55S4.3 glass were investigated. The bond length for Si-O and P-O was determined to be 1.61 Å and 1.49 Å, respectively. The O-Si-O and O-P-O bond angle distributions are both centered at 109 degrees supporting the tetrahedron of the glass formers oxygen coordination. The coordination of Si and P remain 4.0 and does not change with composition. As for boron, two species ([3]B and [4]B) with different structure features can be clearly observed. Boron coordination number, on the other hand, decreases slightly with four-fold coordinated boron oxide fraction from 38% for 25B to 34% for 100B. Also, Ca^{2+} and Sr^{2+} prefer to gather around [PO$_4$] group to create NBO, similar to those found in 45S5 and other bioactive glasses. B_2O_3/SiO_2 substitution leads to an increase of average bridging oxygen around three glass former ions, resulting the increase of overall glass network connectivity. Polyhedral connection distribution results shown that silicon and boron as main components in glasses tend to mixed with each other to form the glass network structure together. The connection probability of [SiO$_4$]-[SiO$_4$] and [SiO$_4$]-[BO$_x$] decreased as the increase of B_2O_3, which leads to an expectation that the B_2O_3/SiO_2 substitution in 55S4.3 would result an increase of glass dissolution. Glass ring size shown a wide distribution range due to the high concentration of glass modifiers (40.9 mol% in total), and adding boron in to silicate glass leads to an increase of ring size of 6~15. Ion diffusion properties derived from MSD calculation was also found to be quite sensitive to glass composition change. In high temperature range (above

T_g), a decrease of E_a for all the ions (especially glass former ions) was observed with B_2O_3/SiO_2 substitution, which should related to the higher diffusion coefficient in glass melts for B ion as compare to that for Si ion. Moreover, these ion diffusion behavior changes in glass melts provides an explanation for the DSC determined decrease of T_g with B_2O_3/SiO_2 substitution. At low temperature range (below T_g), the E_a for modifier ions were increased with B_2O_3/SiO_2 substitution, which can be related to the increase of glass network connectivity. The change of bioactivity with B_2O_3/SiO_2 substitution was considered to be related to the change of pH value and release of boric acid to the solution. In addition, the inability to form silica gel due to fast dissolution can be the main reason why slower rate of HAp formation with higher boron oxide in the glass composition.

Acknowledgements:

References

1   L. L. Hench, The story of Bioglass®, *J. Mater. Sci. Mater. Med.*, 2006, **17**, 967–978.

2   J. R. Jones, D. S. Brauer, L. Hupa and D. C. Greenspan, Bioglass and Bioactive Glasses and Their Impact on Healthcare, *Int. J. Appl. Glas. Sci.*, 2016, **7**, 423–434.

3   P. Wray, 'Cotton candy' that heals ?, *Am. Ceram. Soc. Bull.*, 2010, **90**, 25–29.

4   S. B. Jung, in *Bio-Glasses*, John Wiley & Sons, Ltd, Chichester, UK, 2012, pp. 75–95.

5   J. E. Gough, J. R. Jones and L. L. Hench, Nodule formation and mineralisation of human primary osteoblasts cultured on a porous bioactive glass scaffold, *Biomaterials*, 2004, **25**, 2039–2046.

6   J. R. Jones, L. M. Ehrenfried and L. L. Hench, Optimising bioactive glass scaffolds for bone tissue engineering, *Biomaterials*, 2006, **27**, 964–973.

7   J. R. Jones, O. Tsigkou, E. E. Coates, M. M. Stevens, J. M. Polak and L. L. Hench, Extracellular matrix formation and mineralization on a phosphate-free porous bioactive glass scaffold using primary human osteoblast (HOB) cells, *Biomaterials*, 2007, **28**, 1653–1663.

8   A. Yao, D. Wang, W. Huang, Q. Fu, M. N. Rahaman and D. E. Day, In vitro bioactive characteristics of borate-based glasses with controllable degradation behavior, *J. Am. Ceram. Soc.*, 2007, **90**, 303–306.

9   W. Huang, D. E. Day, K. Kittiratanapiboon and M. N. Rahaman, Kinetics and mechanisms of the conversion of silicate (45S5), borate, and borosilicate glasses to hydroxyapatite in dilute phosphate solutions, *J. Mater. Sci. Mater. Med.*, 2006, **17**, 583–596.

10   A. M. Deliormanlı and M. N. Rahaman, Direct-write assembly of silicate and borate bioactive glass scaffolds for bone repair, *J. Eur. Ceram. Soc.*, 2012, **32**, 3637–3646.

11   H. Fu, Q. Fu, N. Zhou, W. Huang, M. N. Rahaman, D. Wang and X. Liu, In vitro evaluation of borate-based bioactive glass scaffolds prepared by a polymer foam replication method, *Mater. Sci. Eng. C*, 2009, **29**, 2275–2281.

12   L. Bi, M. N. Rahaman, D. E. Day, Z. Brown, C. Samujh, X. Liu, A. Mohammadkhah, V. Dusevich, J. D. Eick and L. F. Bonewald, Effect of bioactive borate glass microstructure on bone regeneration, angiogenesis, and hydroxyapatite conversion in a rat calvarial defect model, *Acta Biomater.*, 2013, **9**, 8015–8026.

13   R. F. Brown, M. N. Rahaman, A. B. Dwilewicz, W. Huang, D. E. Day, Y. Li and B. S. Bal, Effect of borate glass composition on its conversion to hydroxyapatite and on the proliferation of MC3T3-E1 cells, *J. Biomed. Mater. Res. - Part A*, 2009, **88**, 392–400.

14   X. Liu, Z. Xie, C. Zhang, H. Pan, M. N. Rahaman, X. Zhang, Q. Fu and W. Huang, Bioactive borate glass scaffolds: In vitro and in vivo evaluation for use as a drug delivery system in the treatment of bone infection, *J. Mater. Sci. Mater. Med.*, 2010, **21**, 575–582.

15   X. Zhang, W. Jia, Y. Gu, W. Xiao, X. Liu, D. Wang, C. Zhang, W. Huang, M. N.

Rahaman, D. E. Day and N. Zhou, Teicoplanin-loaded borate bioactive glass implants for treating chronic bone infection in a rabbit tibia osteomyelitis model, *Biomaterials*, 2010, **31**, 5865–5874.

16   D. Arcos, C. V. Ragel and M. Vallet-Regí, Bioactivity in glass/PMMA composites used as drug delivery system, *Biomaterials*, 2001, **22**, 701–708.

17   Z. R. Domingues, M. E. Cortés, T. A. Gomes, H. F. Diniz, C. S. Freitas, J. B. Gomes, A. M. C. Faria and R. D. Sinisterra, Bioactive glass as a drug delivery system of tetracycline and tetracycline associated with β-cyclodextrin, *Biomaterials*, 2004, **25**, 327–333.

18   A. A. Gorustovich, J. M. P. López, M. B. Guglielmotti and R. L. Cabrini, Biological performance of boron-modified bioactive glass particles implanted in rat tibia bone marrow, *Biomed. Mater.*, 2006, **1**, 100–105.

19   Y. Hong, X. Chen, X. Jing, H. Fan, Z. Gu and X. Zhang, Fabrication and drug delivery of ultrathin mesoporous bioactive glass hollow fibers, *Adv. Funct. Mater.*, 2010, **20**, 1503–1510.

20   X. Cui, C. Zhao, Y. Gu, L. Li, H. Wang, W. Huang, N. Zhou, D. Wang, Y. Zhu, J. Xu, S. Luo, C. Zhang and M. N. Rahaman, A novel injectable borate bioactive glass cement for local delivery of vancomycin to cure osteomyelitis and regenerate bone, *J. Mater. Sci. Mater. Med.*, 2014, **25**, 733–745.

21   M. Vallet-Regi, A. Rámila, R. P. Del Real and J. Pérez-Pariente, A new property of MCM-41: Drug delivery system, *Chem. Mater.*, 2001, **13**, 308–311.

22   M. Vallet-Regí, F. Balas and D. Arcos, Mesoporous materials for drug delivery, *Angew. Chemie - Int. Ed.*, 2007, **46**, 7548–7558.

23   P. Zapol, H. He, K. D. Kwon and L. J. Criscenti, First-Principles Study of Hydrolysis Reaction Barriers in a Sodium Borosilicate Glass, *Int. J. Appl. Glas. Sci.*, 2013, **4**, 395–407.

24   Y. Yu and M. Edén, Structure–composition relationships of bioactive borophosphosilicate glasses probed by multinuclear [11] B, [29] Si, and [31] P solid state NMR, *RSC Adv.*, 2016, **6**,

101288–101303.

25   N. Stone-Weiss, E. M. Pierce, R. E. Youngman, O. Gulbiten, N. J. Smith, J. Du and A. Goel, Understanding the structural drivers governing glass-water interactions in borosilicate based model bioactive glasses, *Acta Biomater.*, 2017, **65**, 436–449.

26   J. K. Christie and A. Tilocca, Integrating biological activity into radioisotope vectors: molecular dynamics models of yttrium-doped bioactive glasses, *J. Mater. Chem.*, 2012, **22**, 12023.

27   J. Du and Y. Xiang, Effect of strontium substitution on the structure, ionic diffusion and dynamic properties of 45S5 Bioactive glasses, *J. Non. Cryst. Solids*, 2012, **358**, 1059–1071.

28   Y. Xiang and J. Du, Effect of strontium substitution on the structure of 45S5 bioglasses, *Chem. Mater.*, 2011, **23**, 2703–2717.

29   A. Tilocca, A. N. Cormack and N. H. De Leeuw, The structure of bioactive silicate glasses: New insight from molecular dynamics simulations, *Chem. Mater.*, 2007, **19**, 95–103.

30   A. C. T. van Duin, A. Strachan, S. Stewman, Q. Zhang, X. Xu and W. A. Goddard, ReaxFF SiO Reactive Force Field for Silicon and Silicon Oxide Systems, *J. Phys. Chem. A*, 2003, **107**, 3803–3811.

31   A. S. Côté, A. N. Cormack and A. Tilocca, Influence of Calcium on the Initial Stages of the Sol–Gel Synthesis of Bioactive Glasses, *J. Phys. Chem. B*, 2016, **120**, 11773–11780.

32   X. Lu, L. Deng, P.-H. Kuo, M. Ren, I. Buterbaugh and J. du, Effects of boron oxide substitution on the structure and bioactivity of SrO-containing bioactive glasses, *J. Mater. Sci.*, 2017, **52**, 8793–8811.

33   L. Deng and J. Du, Development of effective empirical potentials for molecular dynamics simulations of the structures and properties of boroaluminosilicate glasses, *J. Non. Cryst. Solids*, 2016, **453**, 177–194.

34   M. Ren, L. Deng and J. Du, Bulk, surface structures and properties of sodium borosilicate

and boroaluminosilicate nuclear waste glasses from molecular dynamics simulations, *J. Non. Cryst. Solids*, 2017, **476**, 87–94.

35   W. Cao and L. L. Hench, Bioactive materials, *Ceram. Int.*, 1996, **22**, 493–507.

36   W. Smith and T. R. Forester, DL_POLY_2.0: A general-purpose parallel molecular dynamics simulation package, *J. Mol. Graph.*, 1996, **14**, 136–141.

37   L. Deng and J. Du, Effects of system size and cooling rate on the structure and properties of sodium borosilicate glasses from molecular dynamics simulations, *J. Chem. Phys.*, 2018, **148**, 24504.

38   J. M. D. Lane, Cooling rate and stress relaxation in silica melts and glasses via microsecond molecular dynamics, *Phys. Rev. E - Stat. Nonlinear, Soft Matter Phys.*, 2015, **92**, 1–8.

39   A. Tilocca, Cooling rate and size effects on the medium-range structure of multicomponent oxide glasses simulated by molecular dynamics, *J. Chem. Phys.*, 2013, **139**, 114501.

40   L. R. Corrales and J. Du, Thermal kinetics of glass simulations, *Phys. Chem. Glas.*, 2005, **46**, 420–424.

41   M. Ren and J. Du, Structural Origin of the Thermal and Diffusion Behaviors of Lithium Aluminosilicate Crystal Polymorphs and Glasses, *J. Am. Ceram. Soc.*, 2016, **99**, 2823–2833.

42   L. Brewer, R. H. Lamoreaux, P. H. Poole, P. F. McMillan and G. H. Wolf, Computer simulations of silicate melts, *Rev. Mineral. Geochemistry*, 1995, **32**, 563–616.

43   M. Guerette and L. Huang, In-situ Raman and Brillouin light scattering study of the international simple glass in response to temperature and pressure, *J. Non. Cryst. Solids*, 2015, **411**, 101–105.

44   C.-C. Lin, S.-F. Chen, K. S. Leung and P. Shen, Effects of CaO/P2O5 ratio on the structure and elastic properties of SiO2–CaO–Na2O–P2O5 bioglasses, *J. Mater. Sci.*

Mater. Med., 2012, **23**, 245–258.

45   J. Massera, S. Fagerlund, L. Hupa and M. Hupa, Crystallization Mechanism of the Bioactive Glasses, 45S5 and S53P4, *J. Am. Ceram. Soc.*, 2012, **95**, 607–613.

46   J. Massera and L. Hupa, Influence of SrO substitution for CaO on the properties of bioactive glass S53P4, *J. Mater. Sci. Mater. Med.*, 2014, **25**, 657–668.

47   K. Xie, L. L. Zhang, X. Yang, X. Wang, G. Yang, L. L. Zhang, Y. He, J. Fu, Z. Gou, H. Shao, Y. He, J. Fu and Z. Gou, Preparation and Characterization of Low Temperature Heat-Treated 45S5 Bioactive Glass-Ceramic Analogues, *Biomed. Glas.*, 2015, **1**, 80–92.

48   X. Yang, L. Zhang, X. Chen, X. Sun, G. Yang, X. Guo, H. Yang, C. Gao and Z. Gou, Incorporation of B2O3 in CaO-SiO2-P2O5 bioactive glass system for improving strength of low-temperature co-fired porous glass ceramics, *J. Non. Cryst. Solids*, 2012, **358**, 1171–1179.

49   J. Du and A. N. Cormack, The medium range structure of sodium silicate glasses: A molecular dynamics simulation, *J. Non. Cryst. Solids*, 2004, **349**, 66–79.

50   J. Du and A. N. Cormack, Molecular Dynamics Simulation of the Structure and Hydroxylation of Silica Glass Surfaces, *J. Am. Ceram. Soc.*, 2005, **88**, 2532–2539.

51   L. Pedesseau, S. Ispas and W. Kob, First-principles study of a sodium borosilicate glass-former. II. the glass state, *Phys. Rev. B - Condens. Matter Mater. Phys.*, 2015, **91**, 1–18.

52   L. Pedesseau, S. Ispas and W. Kob, First-principles study of a sodium borosilicate glass-former. I. the liquid state, *Phys. Rev. B - Condens. Matter Mater. Phys.*, 2015, **91**, 1–14.

53   R.A.Smith, Boron in glass and glass making, *J. Non. Cryst. Solids*, 1986, **84**, 421–432.

54   M. M. Smedskjaer, R. E. Youngman, S. Striepe, M. Potuzak, U. Bauer, J. Deubener, H. Behrens, J. C. Mauro and Y. Yue, Irreversibility of pressure induced boron speciation change in glass., *Sci. Rep.*, 2014, **4**, 3770.

55   A. Tilocca, Dynamical descriptors of bioactivity: a correlation between chemical durability and ion migration in biodegradable glasses, *Phys. Chem. Chem. Phys.*, 2017, **19**,

6334–6337.

56   Y. Xiang, J. Du, M. M. Smedskjaer and J. C. Mauro, Structure and properties of sodium aluminosilicate glasses from molecular dynamics simulations., *J. Chem. Phys.*, 2013, **139**, 44507.

57   H. Mehrer, A. W. Imre and E. Tanguep-Nijokep, Diffusion and ionic conduction in oxide glasses, *J. Phys. Conf. Ser.*, 2008, **106**, 12001.

58   H. Lu and R. Dieckmann, Sodium tracer diffusion in glasses of the type (CaO·Al2O3)x(2SiO2)1−x, *J. Non. Cryst. Solids*, 2007, **353**, 2528–2544.

59   X. Wu, R. E. Youngman and R. Dieckmann, Sodium tracer diffusion and11B NMR study of glasses of the type (Na2O)0.17(B2O3)x(SiO2)0.83-x, *J. Non. Cryst. Solids*, 2013, **378**, 168–176.

60   M. Neyret, M. Lenoir, A. Grandjean, N. Massoni, B. Penelon and M. Malki, Ionic transport of alkali in borosilicate glass. Role of alkali nature on glass structure and on ionic conductivity at the glassy state, *J. Non. Cryst. Solids*, 2015, **410**, 74–81.

61   S. Murugavel, C. Vaid, V. S. Bhadram and C. Narayana, Ion Transport Mechanism in Glasses: Non-Arrhenius Conductivity and Nonuniversal Features, *J. Phys. Chem. B*, 2010, **114**, 13381–13385.

62   P. K. Gupta and J. C. Mauro, Composition dependence of glass transition temperature and fragility. I. A topological model incorporating temperature-dependent constraints, *J. Chem. Phys.*, 2009, **130**, 94503.

63   P. G. Debenedetti and F. H. Stillinger, Supercooled liquids and the glass transition, *Nature*, 2001, **410**, 259–267.

64   A. Tilocca, A. N. Cormack and N. H. de Leeuw, The formation of nanoscale structures in soluble phosphosilicate glasses for biomedical applications: MD simulations, *Faraday Discuss.*, 2007, **136**, 45.

65   M. Edén, The split network analysis for exploring composition--structure correlations in

multi-component glasses: I. Rationalizing bioactivity-composition trends of bioglasses, *J. Non. Cryst. Solids*, 2011, **357**, 1595–1602.

66   D. S. Brauer, Bioactive glasses—structure and properties, *Angew. Chemie Int. Ed.*, 2015, **54**, 4160–4181.

67   R. Hill, An alternative view of the degradation of bioglass, *J. Mater. Sci. Lett.*, 1996, **15**, 1122–1125.

68   X. Liu, W. Huang, H. Fu, A. Yao, D. Wang, H. Pan, W. W. Lu, X. Jiang and X. Zhang, Bioactive borosilicate glass scaffolds: in vitro degradation and bioactivity behaviors, *J. Mater. Sci. Mater. Med.*, 2009, **20**, 1237–1243.

69   P. N. De Aza, F. Guitian, A. Merlos, E. Lora-Tamayo and S. De Aza, Bioceramics—simulated body fluid interfaces: pH and its influence of hydroxyapatite formation, *J. Mater. Sci. Mater. Med.*, 1996, **7**, 399–402.